Journal of the European Ceramic Society 7 (1991) 155–163

Mechanical Properties of Injection Moulding Suspensions as a Function of Ceramic Volume Fraction and Temperature

T. Zhang & J. R. G. Evans

Department of Materials Technology, Brunel University, Uxbridge, Middlesex UB8 3PH, UK

(Received 3 September 1990; accepted 5 November 1990)

Abstract

The elastic modulus of ceramic injection moulding compositions with ceramic volume fractions from 0 to 0·56 were measured in the temperature range from 20°C to the softening point of 144°C. The uniaxial fracture strength of the most concentrated suspension was measured in the same temperature range. Poisson's ratio was obtained by a strain gauge method in which the electrical heating effect of the gauge was controlled. The results are compared with model predictions in order that such data can be obtained for diverse suspensions from a minimum of measurements. Such results are necessary for the analysis of residual stress and hence cracking during the solidification stage of ceramic injection moulding.

Der Elastizitätsmodul keramischer Spritzgußmassen mit einem keramischen Volumenanteil von 0 bis 0·56 wurde im Temperaturbereich von 20°C bis zum Erweichungspunkt bei 144°C gemessen. Die Zugfestigkeit des Materials mit dem höchsten Feststoffanteil wurde im gleichen Temperaturbereich gemessen. Die Querdehnungszahl wurde mittels Dehnungsmeßstreifen bestimmt, wobei die elektrische Aufheizung des Streifens kontrolliert wurde. Die Ergebnisse werden mit Modellrechnungen vergleichen, damit derartige Daten für verschiedene Suspensionen mit minimalem Meßaufwand gewonnen werden können. Diese Daten werden benötigt, um die beim Spritzgiessen während des Erhärtens auftretenden Restspannungen zu beurteilen und die damit verbundene Rißbildung zu vermeiden.

On a mesuré le module élastique de mélanges destinés au moulage par injection possédant des teneurs en céramique allant de 0 à 0·56, dans un intervalle de températures allant de 20 à 144°C (point de ramolissement). La résistance à la rupture uniaxiale des suspensions les plus concentrées à été mesurée dans la même gamme de températures. Le coefficient de poisson a été estimé à l'aide d'une méthode de jauge de tension dans laquelle l'effet d'échauffement électrique de la jauge était contrôlé. On compare les résultats obtenus avec les prédictions des modèles de façon à ce que de telles données puissent être obtenues pour diverses suspensions à partir d'un minimum de mesures. Ces résultats sont nécessaires pour l'analyse des contraintes résiduelles et, par conséquent pour celle de la fissuration pouvant se produire lors de l'étape de solidification des céramiques élaborées par moulage par injection.

1 Introduction

The defects which originate in large ceramic components prepared by injection moulding can be related in part to the non-uniform shrinkage which takes place at the solidification stage.[1,2] They take the form of voids which result from the fall in pressure as occluded liquid solidifies or alternatively cracks which originate from stresses developed during solidification. The effects of material properties and machine conditions on these defects can be explored using computer programs which model the solidification stage.[3] Such models require a large number of material properties for ceramic suspensions, including thermal diffusivity, equation of state and mechanical properties. Considerable experimental work is therefore needed to obtain meaningful values of these properties before computer modelling can be used. Previous work has shown how thermal diffusivity and equation of state can be predicted from a minimum of experimentation by using ceramic volume fraction dependence laws and group contributions for organic

Journal of the European Ceramic Society 0955-2219/91/$3.50 © 1991 Elsevier Science Publishers Ltd, England. Printed in Great Britain

species.[4,5] The present work extends this approach for the acquisition of mechanical properties of ceramic suspensions in order that stress distributions in simple shapes can be predicted.

2 Experimental Details

2.1 Preparation of suspension and samples

The alumina was grade RA6 and was kindly donated by Alcan Chemicals Ltd (Gerrards Cross, UK). The isotactic and atactic polypropylenes were grade GY545M from ICI (Welwyn Garden City, UK) and grade MF5 from APP Chemicals (Salop, UK) respectively. The lubricant was stearic acid from BDH Chemicals (Poole, UK). The ceramic volume fraction in the suspensions is shown in Table 1. The organic vehicle was atactic polypropylene, isotactic polypropylene and stearic acid in the ratios 4:4:1 for all suspensions and the exact alumina volume loading was obtained from 7 or 8 ashing experiments. Premixing used a Henschel high-speed mixer and compounding used a twin-screw extruder following the procedure described previously.[6]

Samples for mechanical property measurement were prepared by using injection moulding or compression moulding. Compositions 1 and 6 were prepared by injection moulding standard tensile test samples (3 mm × 12 mm section) using a Negri Bossi NB90 machine at an injection temperature of 200°C. Compositions 2 to 5 were prepared in the form of 3-mm sheets by compression moulding at temperatures from 180°C to 210°C depending on ceramic volume loading. From these sheets, bars of length 150 mm and width 12 mm were cut.

2.2 Measurement of Poisson's ratio

Poisson's ratio of all the compositions was measured by using a four-point bending method with inner supports separated by 40 mm. The tensile and compressive strains were measured by using GFCA-3-70 strain gauges from Tokyo Sokki Kenkyujo Co., Ltd, with gauge resistance $120 \pm 0{\cdot}5\,\Omega$, gauge length 3 mm and gauge factor 2·12.

Table 1. Volume fraction of alumina

Composition number	Al_2O_3 *(vol.%)*
1	0
2	$24{\cdot}3 \pm 0{\cdot}1$ (7)
3	$40{\cdot}4 \pm 0{\cdot}8$ (7)
4	$49{\cdot}7 \pm 0{\cdot}2$ (8)
5	$51{\cdot}3 \pm 0{\cdot}1$ (7)
6	$56{\cdot}4 \pm 0{\cdot}7$ (8)

95% Confidence limits are given. The number of ashing experiments is given in brackets.

The change in gauge resistance was measured using a Wheatstone bridge constructed from wire wound resistors and supplied by a variable voltage power supply in order that the power dissipated in the gauge could be controlled. The bridge was calibrated using an ENIA steel beam in four-point bending with a section of 6 mm × 30 mm and a length between loading points of 1 m. The knife edges were separated by 200 mm. A dial gauge accurate to 10 μm was used to record the central deflection.

The output and strain were calibrated under bridge supply conditions which were sufficiently low to avoid heating of the polymeric material of composition 1. This was achieved by reducing the bridge supply voltage until the output of the bridge was stable for long periods. Poisson's ratio of the steel beam was also recorded in the strain region 100×10^{-6} to 600×10^{-6} as a check on accuracy.

2.3 Measurement of Young's modulus and strength

The elastic modulus of the suspensions was measured by using a dynamic Rheometrics solids analyser RSAII with three-point bending mode in the temperature range 35°C to 160°C while composition 6 was tested from 0°C to 165°C. A frequency of 6·28 rad s^{-1} and a strain of 500×10^{-6} were used. The samples were 3 mm in thickness, 6–8 mm in width and 55 mm in length and were cut from the samples used for Poisson's ratio measurement. The distance between the outer loading points was 48 mm. The test pieces were annealed at 130°C for 1 h under vacuum. Measurements were made at 4°C steps with a soak time of 1 min after the chamber had reached the set temperature. The load was automatically adjusted after every two measurements.

Young's modulus was also measured using an Instron testing machine (Model 1195) and an extensometer at temperatures from 21°C to 70°C at a cross-head speed of 2 mm min^{-1}. A controlled temperature cabinet was used and samples were held at each temperature for 10 min before testing. The extensometer (Instron Model G51-14MA) had a temperature induced error of 0·3% but since it was reset to zero at each temperature, the manufacturer's quoted error of 5% is superimposed. Values of secant modulus were also obtained from the four-point loading strain gauge assembly by static loading.

The tensile strength of composition 6 was measured by using Instron Model 1195 in the temperature range 20°C to 120°C. The cross-head

speed was 5 mm min^{-1}. The samples were held for 10 min in a fan-assisted oven at the desired temperature before testing. The temperature was measured by a mercury in glass thermometer with accuracy $\pm 0{\cdot}5°C$.

3 Results and Discussion

3.1 Poisson's ratio of particle filled suspensions

The strain in the outermost fibre of the calibration beam calculated from small deflection beam theory was a linear function of output from the bridge in the range 40 to 600 microstrain with a linear regression coefficient of 0·9998. The maximum error introduced by using the linear relation to calculate strain in the range 200–600 microstrain was greatest at low strain and gave rise to a maximum error of 7% in Poisson's ratio. Poisson's ratio for the steel beam measured in the range 200 to 600 microstrain was 0·28 and should be compared with the literature value of 0·27.[7] The power dissipated in the strain gauge was 0·33 mW corresponding to 0·055 kW m^{-2} and was sufficiently low to effect a negligible temperature increase when the gauges were attached to the unfilled organic vehicle (composition 1) which has the lowest thermal diffusivity.

The annealing of injection-moulded ceramic suspensions has been shown to affect thermal expansion coefficient[8] and its effect on Poisson's ratio was determined using composition 6. Poisson's ratio for the unannealed sample was $0{\cdot}286 \pm 0{\cdot}004$ for 30 measurements. After annealing at 130°C for 1 h *in vacuo* the corresponding mean and standard deviations were $0{\cdot}285 \pm 0{\cdot}005$ for five measurements, indicating that annealing has an insignificant effect on Poisson's ratio.

The relationship between ceramic volume loading and Poisson's ratio is shown in Fig. 1. With an increase in ceramic volume loading, the Poisson's ratio decreases as expected. The straight line represents the volumetric law of mixtures taking the Poisson's ratio of alumina as 0·25 after Coble & Kingery.[9] It may be seen that Poisson's ratio for compositions 3 to 6 with ceramic volume loadings of 40 to 56 vol.% was much smaller than those calculated from the volumetric mixing law. The deviation is reflected in the thermal expansion data reported previously.[5] It can be speculated that the deviation is attributable to the volume fraction of adsorbed organic matter which increases as ceramic volume fraction increases.[6] It is well known that immobile polymer adsorbates perturb the mechanical properties of polymer composites.[10] For the

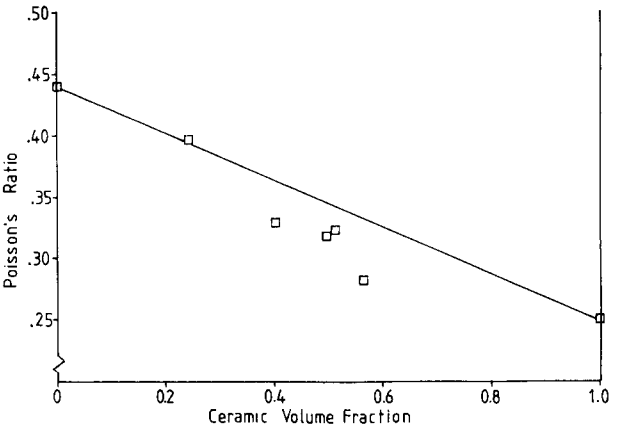

Fig. 1. The effect of ceramic volume fraction on Poisson's ratio.

purposes of quantitative prediction, however, it is of interest to compare the form of the dependence of viscosity on ceramic volume loading for these suspensions. It was found that viscosity approached infinity as particles came into contact at a ceramic volume fraction of about 0·68.[6] Thereafter ceramic volume fraction in the binary system cannot be increased for a given powder.

Thus in Fig. 2 Poisson's ratio is plotted as a function of relative ceramic volume fraction V/V_{max}. The linear relationship is excellent and this method can be used to predict Poisson's ratio of the mixtures to an accuracy of 7%, provided V_{max} is known from viscosity measurements. An analogous argument could be used to explain the effect of ceramic loading on thermal expansion in the solid state.[5]

While it is reasonable to assume that at $V < V_{max}$, dispersed particles are surrounded by an organic phase and that at V_{max} particles make contact, it does not follow that a system of contacting particles presents a Poisson's ratio identical to the bulk. On the one hand, the system of contacting particles

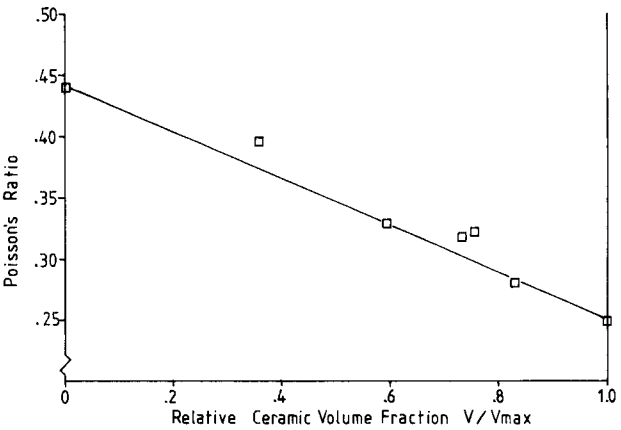

Fig. 2. Poisson's ratio as a function of relative ceramic volume fraction.

could be considered as a porous body with porosity V_p for which[11]

$$v = v_0 - CV_p \quad (1)$$

where v_0 is the Poisson's ratio of the dense ceramic and C is a constant equal to 0·35 for alumina in the range $0 < V_p < 0{\cdot}05$. On the other hand, interstitial space between contacting particles is entirely filled with an organic phase of Poisson's ratio 0·45, which can be expected to increase Poisson's ratio of such a composite. The experimental value at V_{max} remains inaccessible because of the difficulties of fabrication. The approach used in Fig. 2 therefore only has empirical status.

The Poisson's ratio of organic vehicle can itself be estimated by using the volumetric law of mixtures, since the bulk moduli of different organic components are not very large. Poisson's ratio was taken as 0·40 and 0·49 for isotactic polypropylene and atactic polypropylene respectively.[5] If the effect of stearic acid is ignored, this gives a predicted value of 0·447 which, compared with the experimental results, is in error by 2%.

The dependence of Poisson's ratio on strain is shown in Fig. 3. It is seen that under low strains (less than 900×10^{-6}) the effect of strain on Poisson's ratio is very small.

3.2 Young's modulus measurements

The nonlinear relationship between load and deflection for organic vehicles based on semi-crystalline polymers or waxes complicates the stress analysis in mouldings. Furthermore, the time-dependent effects in a polymer with very low crystallinity complicate measurement. Three methods were therefore used and are compared. Conventional stress–strain curves in uniaxial tension were obtained by the standard method[12] for composition 6. Static loading measurement in four-point bending using strain gauges offers a simple procedure which gives Poisson's ratio and secant modulus and was used for all compositions at room temperature. The dynamic modulus at low frequency (1 Hz) was also obtained in three-point bending mode over wide temperature and ceramic volume loading ranges.

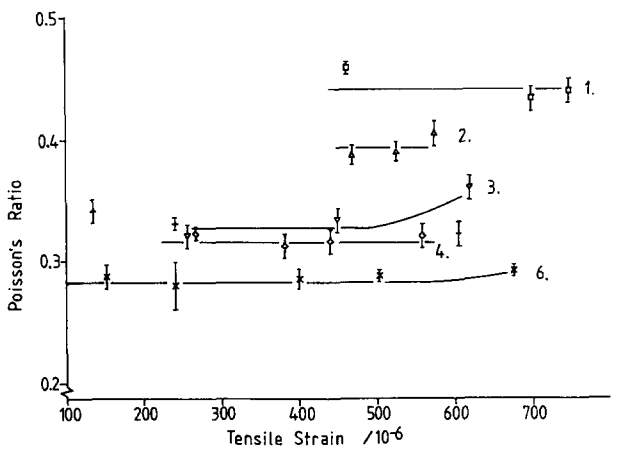

Fig. 3. The effect of strain on Poisson's ratio.

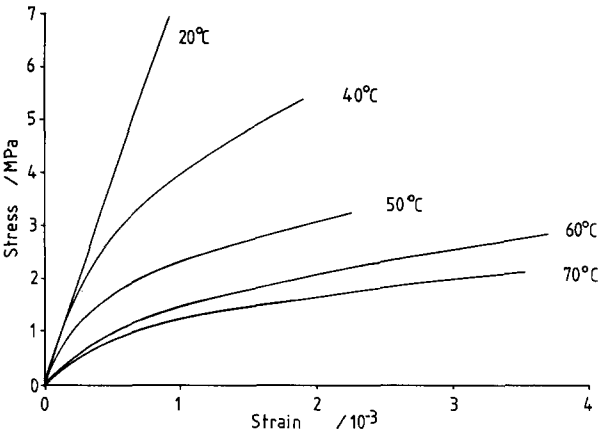

Fig. 4. Tensile deformation curves for composition 6 at 20–70°C.

Figure 4 shows tensile stress–strain curves for composition 6 at temperatures up to 70°C (the limit for the extensometer). These fit the general relationship

$$\sigma = B\varepsilon^n \quad (2)$$

and the values of B and n obtained from a least squares regression analysis of eqn (2) are shown in Table 2. At room temperature the composite approximates to a linear elastic solid, but the load–deflection curves deviate from linearity significantly as the temperature rises and this is reflected in a decreasing value of n.

The secant moduli obtained from static loading experiments in four-point bending with strain gauges are shown in Table 3 for compositions 1–6 at room temperature. The secant modulus obtained from the uniaxial tensile tests at 500 microstrain for composition 6 at room temperature is given for comparison. The method is simple to set up but offers a less exact result because at about 400

Table 2. Results of uniaxial tensile tests for composition 6 at various temperatures

Temperature (°C)	*B* (GPa)	*n*	*Regression coefficient*
20	7·66	1·00	1
40	0·40	0·66	0·989
50	0·17	0·63	0·991
60	0·20	0·74	0·986
70	0·08	0·64	0·994

Table 3. Secant moduli at room temperature from static loading

Composition number	*Secant modulus (GPa) 500 με)*
1	0·6
2	1·1
3	2·6
4	2·9
5	5·7
6	7·9
6[a]	7·7

[a] From uniaxial tensile tests.

microstrain time-dependent deformation is noticeable. It is difficult to apply to compositions wherein time-dependent deformation occurs or at elevated temperatures.

The complete variation in elastic modulus with temperature and composition was obtained from dynamic mechanical analysis in three-point bending at 1 Hz and the results are shown in Fig. 5. Up to 140°C, which represents the softening point, the logarithm of Young's modulus decays linearly with temperature. The curves can be approximated by a general expression:

$$\log E = \log E_0 - bT \qquad (3)$$

and the constants E_0 and b are given in Table 4 together with the linear regression coefficient for the logarithmic straight line in the temperature range 40–140°C (0–140°C for composition 6). Above 140°C the crystalline fraction of the organic vehicle melts and the modulus decreases steeply.

It can be seen that as the ceramic volume fraction increases, the softening temperatures increase slightly. The addition of 56 vol.% ceramic increases the softening point of the unfilled polymer by about 10°C. A similar effect is seen in the elevation of glass transition temperature in filled polymers and is attributed to the influence of high-energy internal surfaces on the conformation of adjacent polymer molecules.[13] The elastic moduli for composition 6, measured by different methods, are compared in Table 5. At 20°C this material is approximately linearly elastic and hence the secant and tangent moduli coincide. The strain gauge secant modulus is similar for the same reason showing that this simple

Table 4. The dependence of Young's modulus on temperature ($\log E = \log E_0 - bT$; $35 < T < 140$°C)

Composition	*log E_0*	*b*	*Regression coefficient*
1	8·86	0·0127	−0·987
2	9·37	0·0130	−0·997
3	9·58	0·0126	−0·999
4	9·73	0·0136	−0·999
5	9·93	0·0143	−0·999
6	10·29	0·0132	−0·999

Table 5. Comparison of elastic modulus determinations for composition 6

Temperature (°C)	*Elastic modulus (GPa)*			
	Uniaxial tension (tangent)	*Uniaxial tension (secant (500 με)*	*Strain gauge (secant 500–700 με)*	*Dynamic (1 Hz, 500 με)*
20	7·7	7·7	7·8	8·3
40	6·4	5·2	—	6·0
50	4·9	3·0	—	4·4
60	1·7	1·6	—	3·2
70	1·5	1·3	—	2·4

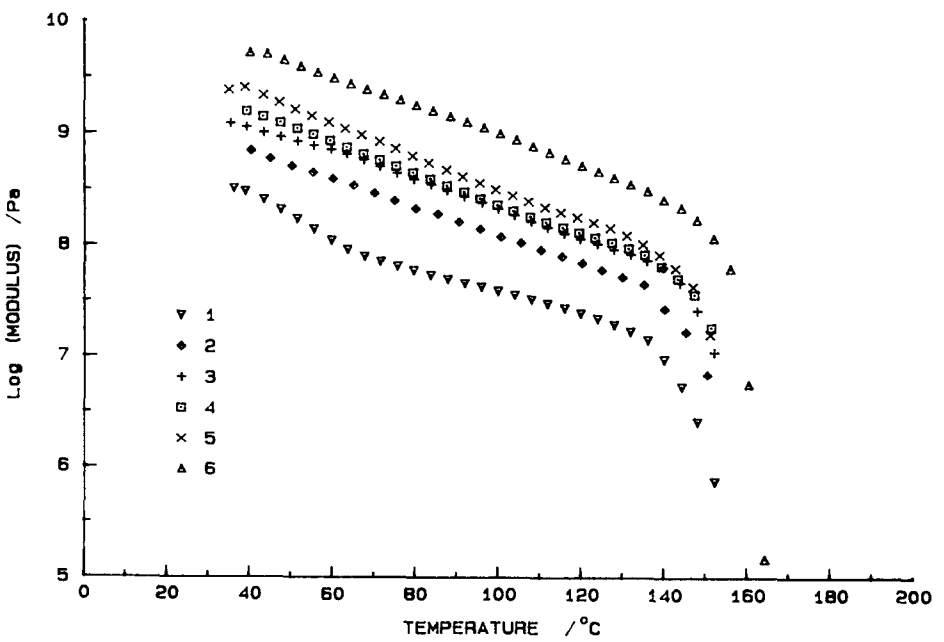

Fig. 5. Dynamic elastic modulus as a function of temperature for compositions 1–6 (frequency, 1 Hz).

test can give a good estimate of elastic modulus as well as Poisson's ratio under the conditions discussed. The dynamic elastic moduli at each temperature are slightly larger than the secant moduli under uniaxial tension for two reasons. In the first place they are measured at a higher strain rate of $1000 \times 10^{-6} s^{-1}$ as opposed to $290 \times 10^{-6} s^{-1}$ and the organic vehicle is a strain rate-sensitive polymer. In the second place, they are measured in a bending mode on materials which are not linearly elastic (Table 2). Hence the stress does not change linearly from the outer fibre of the beam to the neutral axis. The modulus is calculated from the apparent stress in the outermost fibre assuming linear elasticity, σ_{max}, at a fixed strain of 500×10^{-6} and compared with the 500×10^{-6} secant modulus in uniaxial tension at the same strain in Table 5. The true stress σ'_{max} in the outer fibre is therefore smaller than for a linear elastic material for a given load according to Ref. 14:

$$\sigma'_{max} = \frac{n+2}{3}\sigma_{max} \quad (4)$$

so that the true modulus is lower than the apparent modulus. The difference is accentuated at higher temperatures as n deviates further from unity.

3.3 The volume fraction dependence of elastic modulus

There are a number of models for the shear modulus G^* and bulk modulus K^* of multiphase materials. The most widely used give the upper and lower bounds and were derived by Hashin & Shtrikman:[15]

$$G_l^* = G_1 + \frac{V}{\frac{1}{G_2 - G_1} + \frac{6(K_1 + 2G_1).(1-V)}{5G_1(3K_1 + 4G_1)}} \quad (5a)$$

$$G_u^* = G_2 + \frac{1-V}{\frac{1}{G_1 - G_2} + \frac{6(K_2 + 2G_2)}{5G_2(3K_2 + 4G_2)}.V} \quad (5b)$$

where V is the volume loading of the dispersed phase. Subscripts u and l refer to the upper and lower bounds respectively. The shear modulus G and bulk modulus K can be expressed in terms of Young's modulus:

$$G = E/2(1+v) \quad \text{and} \quad K = E/3\,(1-2v) \quad (6)$$

where v is the Poisson's ratio, which has been discussed above. Equations (5a) and (5b) can be used for predicting the upper and lower bounds for

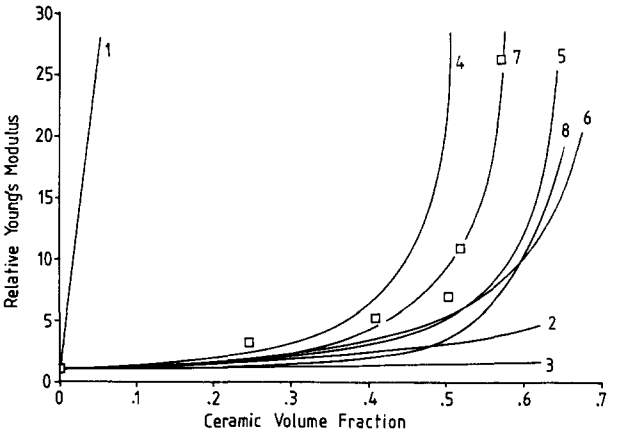

Fig. 6. Relative dynamic elastic modulus as a function of ceramic volume loading (frequency, 1 Hz; temperature, 40°C). 1, eqn (5b); 2, eqn (5a) and eqn (11); 3, eqn (7); 4, eqn (8) ($V_m = \pi/6$); 5, eqn (8) ($V_m = 0{\cdot}68$); 6, eqn (9); 7, eqn (12) ($V_m = 0{\cdot}68$, $C = 0{\cdot}25$); 8, eqn (12) ($V_m = 0{\cdot}68$, $C = 0{\cdot}70$).

Young's modulus of suspensions having different ceramic volume loading provided the variation in Poisson's ratio is incorporated.

The usefulness of such predictive models is shown in Fig. 6 wherein the relative elastic moduli are calculated from the best straight lines in Fig. 5. The objective here is to obtain analytical expressions for elastic modulus as a function of temperature and ceramic volume fraction. It can be seen that the curve for the unfilled organic vehicle is not perfectly linear but shows a transition at about 60°C which corresponds to the melting of the stearic acid component of the blend and was previously seen in the thermal expansion curve for this composition (5). The transition cannot be detected at higher volume loadings and this may be partly the result of interfacial factors. It means that relative modulus calculated at different temperatures is not constant and this effect is shown in Fig. 7 where the relative modulus is found from data points at individual temperatures. However, for the purpose of computer modelling of stresses in mouldings, the generalised eqn (3) is preferable.

The Young's modulus of alumina was taken as $380\ GN\ m^{-2}$.[16] It is seen that the upper bound is far away from the experimental results. This arises because the Young's modulus of alumina is much larger than that of the organic binder. The lower bound is much smaller than the experiment results, especially at high volume loadings. The bounds are widely separated because of the large difference in modulus of the constituents and, while reported experimental results generally fall within them, their use is limited if the objective is to predict elastic modulus of ceramic injection moulding suspensions from a knowledge of binder and ceramic properties.

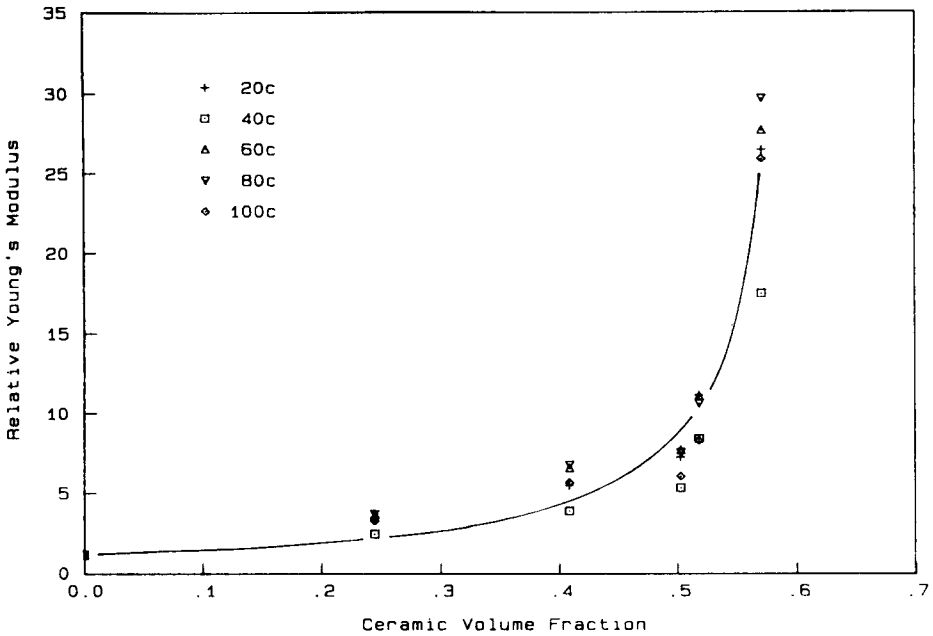

Fig. 7. Relative elastic modulus as a function of volume loading deduced from the data in Fig. 6 at five temperatures. Superimposed is the best predictive curve: eqn (12).

For dilute suspensions, Hashin[17] gives an alternative model

$$\frac{K^*}{K_1} = 1 - \frac{3(1-\nu_1)(1-K_2/K_1)V}{2(1-2\nu_1)+(1+\nu_1)(K_2/K_1)} \tag{7a}$$

which can be simplified as:

$$K^* = K_1 + \frac{(K_2-K_1)V}{1+[(K_2-K_1)/(K_1+\frac{4}{3}G_1)]} \tag{7b}$$

Once again the variation in Poisson's ratio must be incorporated and the curve for eqn (7) is shown in Fig. 6. Although it is close to the experimental results at low volume loadings the deviation is high at high ceramic volume loadings. Hashin[17] also offers a composite spheres model which turns out to be the same as the lower bound in eqn (5a).

For concentrated suspensions based on cubic packing geometry Christensen[18] suggests a volume dependence model for shear moduli:

$$\frac{G}{G_1} = \frac{3\pi}{16[1-(V_{max})^{1/3}]} \tag{8}$$

For cubic packing $V_{max} = \pi/6$ which is slightly smaller than the ceramic volume loading of composition 6. Inserting $V_{max} = 0{\cdot}68$ obtained from viscosity measurements[6] also gives a curve which can be compared with the experimental results (Fig. 6).

The theoretical equations for viscosity and shear modulus should be of the same form; the rate of shear in the viscosity equation being replaced by the shear strain in the modulus equation.[19] Lewis[20] and Nielsen[21] showed that the modulus of composites can be generalised as:

$$\frac{M}{M_1} = \frac{1+ABV}{1-B\psi V} \tag{9}$$

where M is any modulus, shear, Young's or bulk.

$$A = K_e - 1$$

and

$$B = \frac{M_2/M_1 - 1}{M_2/M_1 + A}$$

where K_e is a generalised Einstein coefficient and is 2·5 for spherical inclusions in a liquid. The factor ψ depends on the maximum packing fraction V_m of the filler. It is defined as:

$$\psi = 1 + \left(\frac{1-V_{max}}{V_{max}^2}\right).V \tag{10}$$

The calculated results from eqn (9) are also shown in Fig. 6. They give a better fit to the measured results, but at high volume loading still give a large error. Batchelor & Green[22] estimate the zero shear rate relative viscosity using a series in ascending powers of V up to V^2, and deduce the shear modulus:

$$G/G_1 = 1 + \tfrac{5}{2}V + (5{\cdot}2 \pm 0{\cdot}3)V^2 \tag{11}$$

For high ceramic volume loading, this is also much smaller than the experimental results as shown in Fig. 6 and is nearly the same as Hashin's lower bound.

In the measurement of viscosity of ceramic suspensions it has been shown that Chong's equation with slight modification gives a good fit to

experiment for these ceramic injection moulding compositions:[6]

$$\eta_r = \left(\frac{V_{max} - CV}{V_{max} - V}\right)^2 \quad (12)$$

Using the same equation for Young's modulus, replacing η_r by E/E_0, curves 7 and 8 in Fig. 6 are obtained, which were calculated by taking $V_{max} = 0{\cdot}68$ and $C = 0{\cdot}25$ and $0{\cdot}70$ respectively. It is shown that when $C = 0{\cdot}25$ a good fit to the experimental result is obtained as was the case for viscosity at constant shear stress.[6]

The problem presented by the ceramic volume fraction dependence of elastic modulus is that, while experimental results generally fall within the Hashin & Shtrikman bounds, individual models do not fit data for the wide range of composites studied, especially at high volume loadings. In this work, an equation relevant to viscosity correlates well with the elastic modulus and it will be interesting to see if this is generally true for ceramic injection moulding suspensions. If so it largely eliminates the experimental determination of moduli for different ceramic loadings and diverse ceramics.

3.4 Predicting the Young's modulus of the organic vehicle

Since ceramic injection moulding practitioners use a wide range of organic species, it is of interest to see how effectively Young's modulus for the unfilled materials can be predicted by using group contributions. In this way, elastic modulus as a function of ceramic volume fraction could be estimated with sufficient accuracy for computer modelling from a knowledge of the relative viscosity curve alone. Van Krevelen[23] discusses procedures for the prediction of bulk modulus which can be expressed as:

$$K = \rho\left(\frac{U}{V}\right)^6 \quad (13)$$

where ρ is the density, U is the Rao function and V is the molar volume. For polypropylene the Rao function, which behaves as an additive molar quantity, is $2716\,cm^{10/3}\,mol^{-1}\,s^{-1/3}$ and the molar volume is $48{\cdot}3 \times 10^{-6}\,m^3\,mol^{-1}$. The densities of the atactic and isotactic polypropylene used in this work were 870 and 905 kg m^{-3} respectively. These give predicted bulk moduli and Young's moduli of 2·69 GPa and 0·16 GPa for atactic polypropylene and 2·86 GPa and 1·72 GPa for isotactic polypropylene, respectively. Poisson's ratio was taken as 0·49 and 0·40 for atactic and isotactic polypropylene respectively. If, as a simplification, the stearic acid content, which is small, is considered as atactic polypropylene, application of volumetric law of mixtures gives a Young's modulus of 0·4 GPa at 20°C, which is somewhat lower than the secant modulus of 0·6 GPa from static loading and the 0·7 GPa deduced by short extrapolation in Fig. 5. The use of group contributions therefore appears to be less successful with elastic modulus prediction than was the case for thermal properties of organic vehicle.[4]

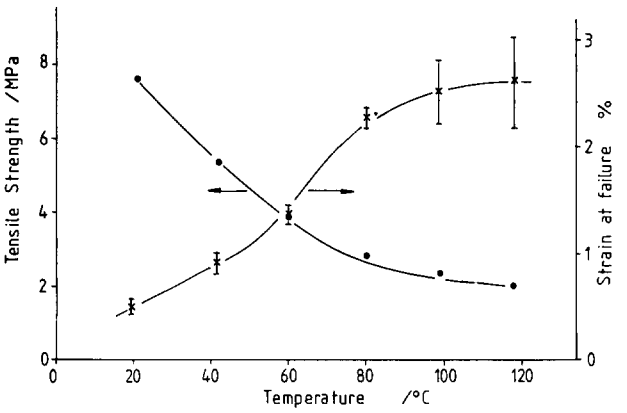

Fig. 8. Tensile strength and strain at failure as a function of temperature for composition 6.

3.5 The temperature dependence of tensile strength

The tensile strength–temperature relationship for composition 6 is shown in Fig. 8. The room-temperature tensile strength was 8 MPa and decreases linearly up to 80°C. The unfilled organic vehicle (composition 1) has a yield stress of 0·47 MPa at 20°C, indicating that the tensile strength increases with ceramic volume fraction. The extension at failure, on the other hand, decreases markedly as expected as ceramic volume fraction increases. Mechanical properties of particulate composites are often attributed to the extent of the acid–base interaction at the interface and experimental justification for this is gradually accumulating.[24–26]

4 Conclusions

Procedures have been established for the estimation of mechanical properties of ceramic injection moulding suspensions for the purpose of computer modelling of stress distribution in mouldings with experimental economy. A static four-point bending jig with strain gauges can be used for Poisson's ratio determination but Poisson's ratio can be predicted from relative ceramic volume fraction, provided V_{max} is known from viscosity measurements. Volumetric rule of mixtures can be used to obtain Poisson's ratio of the organic vehicle. The elastic

modulus of suspensions can be expressed in logarithmic form as a function of temperature below the softening point region. The elastic modulus of suspensions relative to the modulus of the unfilled vehicle can be expressed by a relationship analogous to the relative viscosity–volume loading relation, but conventional expressions for the elastic modulus of particle-filled composites fail to yield accurate predictions, because of the large difference in elastic modulus between ceramic and vehicle. The failure stress, as a function of temperature, requires experimental measurement and cannot be otherwise predicted at present.

Acknowledgement

The authors are grateful to the Science and Engineering Research Council for supporting this work.

References

1. Edirisinghe, M. J. & Evans, J. R. G., Review: fabrication of engineering ceramics by injection moulding. Part I. *Int. J. High Tech. Ceram.*, **2** (1986) 1–31.
2. Edirisinghe, M. J. & Evans, J. R. G., Review: fabrication of engineering ceramics by injection moulding. Part II. *Int. J. High Tech. Ceram.*, **2** (1986) 249–78.
3. Hunt, K. N., Evans, J. R. G. & Woodthorpe, J., Computer modelling of the origin of defects in ceramic injection moulding. Parts I–III, submitted to *J. Mater. Sci.*
4. Zhang, T. & Evans, J. R. G., Thermal properties of ceramic injection moulding suspensions in the liquid and solid states. *J. Eur. Ceram. Soc.*, **5** (1989) 303–9.
5. Zhang, T. & Evans, J. R. G., Thermal expansion and equation of state for ceramic injection moulding suspensions. *J. Eur. Ceram. Soc.*, **6** (1990) 15–21.
6. Zhang, T. & Evans, J. R. G., Predicting the viscosity of ceramic injection moulding suspensions. *J. Eur. Ceram. Soc.*, **5** (1989) 165–72.
7. Mott, R. L., *Machine Elements in Mechanical Design*. Charles E. Merrill Publishing Company, Ohio, 1985, p. 18.
8. Zhang, T. & Evans, J. R. G., Anomalies in the thermal expansion of injection moulded ceramics. *J. Mat. Sci. Lett.*, **9** (1990) 672–4.
9. Coble, R. L. & Kingery, W. O., Effect of porosity on physical properties of sintered alumina. *J. Amer. Ceram. Soc.*, **39** (1956) 377–85.
10. Jancar, J., Kucera, J. & Vesely, P., Some peculiarities in viscoelastic response of heavily filled polypropylene composites. *J. Mater. Sci. Lett.*, **7** (1988) 1377–8.
11. Morrel, R., *Handbook of Properties of Technical and Engineering Ceramics*, Part 2. Her Majesty's Stationery Office, London, 1987, p. 22.
12. ASTM D638-80, Standard test method for tensile properties of plastics. American Society for Testing and Materials, Philadelphia, Part 35, 1980.
13. Howard, G. J. & Shanks, R. A., Influence of filler particles on the mobility of polymer molecules. II. Effect of filler type. *J. Macromol. Sci. Phys.*, **B19** (1981) 167–76.
14. Gere, J. M. & Timoshenko, S. P., *Mechanics of Materials*, 2nd edn. Van Nostrand, Reinhold, Wokingham, UK, 1987, p. 549.
15. Hashin, Z. & Shtrikman, S., A variational approach to the theory of the elastic behaviour of multiphase materials. *J. Mech. Phys. Solids*, **11** (1963) 127–40.
16. Morrel, R., *Handbook of Properties of Technical and Engineering Ceramics*, Part 2, Her Majesty's Stationery Office, London, 1987, p. 21.
17. Hashin, Z., The elastic moduli of heterogeneous materials. *J. Appl. Mech.*, **29** (1962) 143.
18. Christensen, R. M., *Mechanics of Composite Materials*. Wiley, NY, 1979, pp. 61–7.
19. Nielsen, L. E., *Mechanical Properties of Polymers and Composites*, Vol. 2. Marcel Dekker Inc., NY, 1974, pp. 387–405.
20. Lewis, T. B. & Nielsen, L. E., Dynamic mechanical properties of particulate filled composites. *J. Appl. Polymer Sci.*, **14** (1970) 1449–71.
21. Nielsen, L. E., Generalized equation for elastic moduli of composite materials. *J. Appl. Phys.*, **41** (1970) 4626–7.
22. Batchelor, G. K. & Green, J. T., The hydrodynamic interaction of two small freely moving spheres in a linear flow field. *J. Fluid Mech.*, **56** (1972) 375.
23. Van Krevelen, D. W., *Properties of Polymers*. Elsevier, Amsterdam, 1972, pp. 147–64.
24. Manson, J. A. & Williams, J. T., Acid–base interaction between siliceous fillers and polymeric matrices. *Org. Coat. Plastic. Chem.*, **42** (1980) 175–80.
25. Manson, J. A., Lin, J. S. & Tiburcio, A., Some effects of acid–base interactions in polymer composites and coatings. *Org. Coat. Plastic Chem.*, **46** (1982) 121–6.
26. Manson, J. A., Interfacial effects in composites. *Pure Appl. Chem.*, **57** (1985) 1667–8.